Electronic Supplementary Information

Crystalline/amorphous c-NiMo/a-$NiMoO_x$ nanoarrays for urea-assisted energy-saving H_2 production in alkaline seawater

Dongxue Guo*[a], Yi Ping [b], Chuanjiao Wang [b], Changan Hou [b], Danhong Wang*[b]

[a]Academy of National Food and Strategic Reserves Administration, Beijing 100037, China.

[b]TKL of Metal and Molecule Based Material Chemistry, School of Materials Science and Engineering, Nankai University, Tianjin 300350, China.

*Corresponding author.

Email: gdx@ags.ac.cn; dhwang@nankai.edu.cn

Experimental section

Materials

All the chemicals were used as received without further purification. Nickel nitrate hexahydrate ($Ni(NO_3)_2 \cdot 6H_2O$), potassium hydroxide (KOH) and hydrochloric acid (HCl, ca. 36.0 ~ 38.0 % solution in water) were purchased from Aladdin Industrial Co., Ltd. Ammonium molybdate tetrahydrate ($(NH_4)_6Mo_7O_{24} \cdot 4H_2O$) and urea ($CO(NH_2)_2$) were purchased from Shanghai Macklin Biochemical Industrial Co., Ltd. Commercial Ni foam (thickness of 1.0 mm, bulk density 0.32 g cm^{-2}, Tianjin Ailian Co.,Ltd.) was used as a conductive substrate to grow catalyst. Ultrapure Milli-Q water (18.25 MΩ·cm) was used in all experiments. Natural seawater was collected from the East China Sea with a pH of about 8.26 and used directly without further purification.

Characterization

Powder X-ray diffraction (PXRD) spectra were recorded on a Rigaku Smart Lab powder diffractometer equipped with Cu Kα radiation (λ = 1.5418 Å). The morphology of the samples was characterized by a field emission scanning electron microscopy (FE-SEM) (model JSM-7800F). Transmission electron microscopy (TEM) with high resolution mode (HRTEM) and selected area electron diffraction (SAED) pattern were acquired with JEM-2800 (Japan) operating at an accelerating voltage of 200 kV. The elemental mapping of the samples was performed by energy-dispersive X-ray spectroscope (EDX) accessory attached to the TEM. The inductively-coupled plasma optical emission spectrometry (ICP-OES) was performed on Agilent 5110. X-ray photoelectron spectroscopy (XPS) was investigated by using a Thermo ESCALAB

250XI X-ray photoelectron spectrometer. Raman spectra were obtained using a SR-500I-A Raman spectrometer, with an argon ion laser (785 nm) as the excitation light source. The wettability of the electrodes surface was characterized by surveying the contact angles. The X-ray absorption fine structure (XAFS) measurements were tested at the SPring-8 BL14B2 in Japan Synchrotron Radiation Research Institute (JASRI). XAFS data were tested by a fixed-exit double-crystal Si (111) monochromator.

Electrochemical measurements

Electrochemical measurements were carried out by an electrochemical workstation (Ivium V53517, Netherlands) using a standard three-electrode system in 1.0 M KOH, 1.0 M KOH + 0.33 M Urea, 1 M KOH + 0.33 M Urea + seawater, respectively. The working electrode was the c-NiMo/a-$NiMoO_x$ (and other control samples) with a geometric area of 0.49 cm^2. The Hg/HgO (1.0 M KOH) was used as the reference electrode. A Pt plate with an area of 1 cm^{-2} was used as the counter electrode in OER and UOR, while a graphite rod acted as a counter electrode in HER. All the electrochemical measurements were corrected using 90% iR compensation and calibrated to the reversible hydrogen electrode (RHE) using the Nernst equation: $E_{RHE} = E_{Hg/HgO} + 0.098\ V + 0.059 \times PH$. Linear sweep voltammetry (LSV) was conducted with a scan rate of 2 mV s^{-1}. The electrochemical impedance spectroscopy (EIS) was recorded in the region of 100 kHz-0.1 Hz at an amplitude of 10 mV. The electrochemical active surface area (ECSA) was calculated as the following equation: $ECSA = C_{dl}/C_s$. The C_{dl} is the electrochemical double-layer capacitance obtained from CV cycles. The general specific capacitance of C_s in 1.0 M KOH is usually considered

as a constant (0.04 mF cm^{-2}) based on typical reported values. The faradaic efficiency was calculated from the ratio of the produced and theoretical amounts of H_2 by a water drainage method. The overall urea-assisted seawater/freshwater electrolysis were carried out in a H-type electrolyzer cell with c-NiMo/a-$NiMoO_x$ as the anodic electrode and cathodic electrode, and an anion-exchange membrane as the separator.

DFT calculations

We have employed the Vienna Ab Initio Simulation Package (VASP) to perform all the density functional theory (DFT) calculations within the generalized gradient approximation (GGA) using the PBE formulation.[1-3] We have chosen the projected augmented wave (PAW) potentials to describe the ionic cores and take valence electrons into account using a plane wave basis set with a kinetic energy cutoff of 450 eV.[4,5] Partial occupancies of the Kohn-Sham orbitals were allowed using the Gaussian smearing method and a width of 0.05 eV. The on-site corrections (DFT+U) has been applied to the d electrons of Ni atoms (Ueff = 6.2 eV) and Mo atoms (Ueff = 4.4 eV) and by the approach from Dudarev et al.[6] The electronic energy was considered self-consistent when the energy change was smaller than 10^{-5} eV. A geometry optimization was considered convergent when the force change was smaller than 0.02 eV/Å. Grimme's DFT-D3 methodology was used to describe the dispersion interactions.[7]

The adsorption energy (E_{ads}) of adsorbate A was defined as

$$E_{ads} = E_{A/surf} - E_{surf} - E_{A(g)}$$

where $E_{A/surf}$, E_{surf} and $E_{A(g)}$ are the energy of adsorbate A adsorbed on the polyimide, the energy of clean polyimide, and the energy of isolated A molecule in a cubic periodic

box with a side length of 20 Å and a 1×1×1 Monkhorst-Pack k-point grid for Brillouin zone sampling, respectively.

The free energy of a gas phase molecule or an adsorbate on the surface was calculated by the equation G = E + ZPE − TS, where E is the total energy, ZPE is the zero-point energy, T is the temperature in kelvin (298.15 K is set here), and S is the entropy.

Supplementary Figures

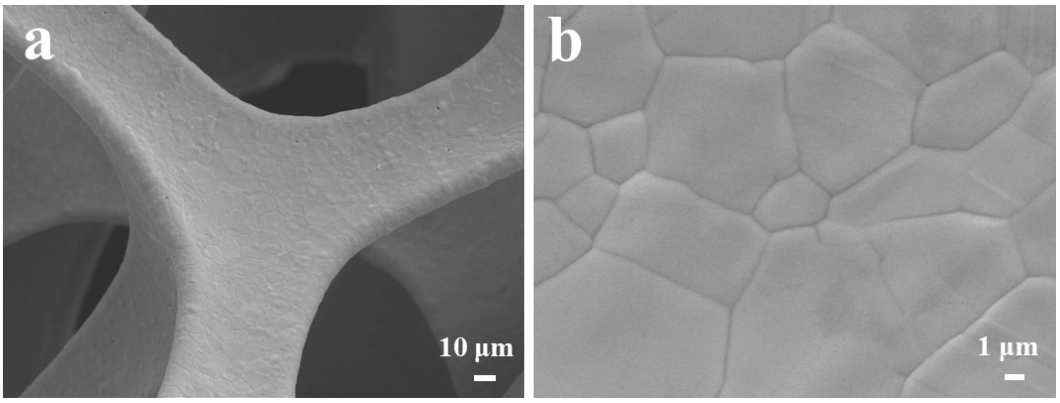

Figure S1. SEM images of (a) low magnification and (b) high magnification of bare Ni foam.

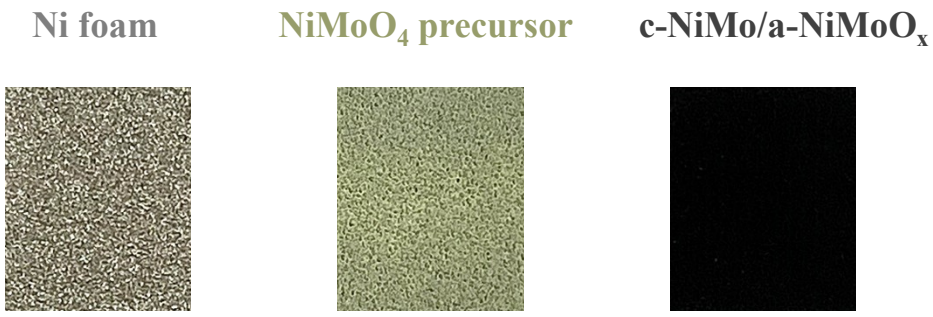

Figure S2. Optical photographs of Ni foam, $NiMoO_4$ precursor and c-NiMo/a-$NiMoO_x$ catalysts.

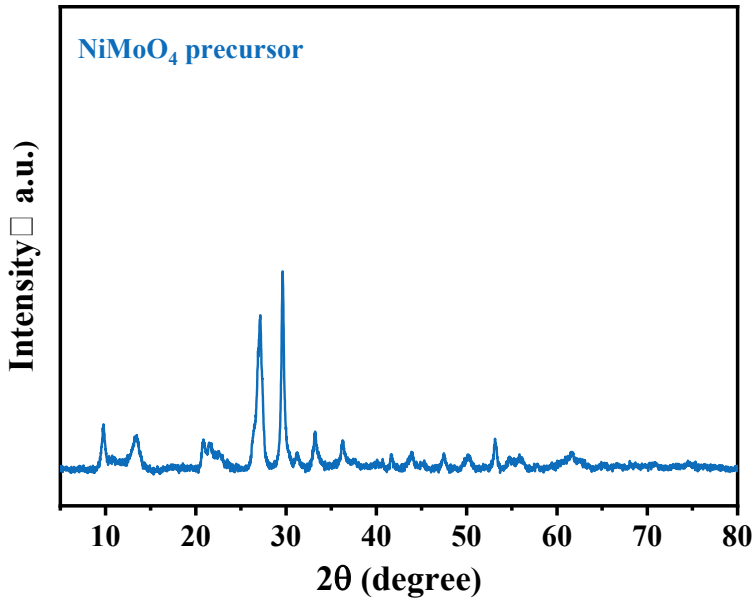

Figure S3. XRD pattern of $NiMoO_4$ precursor.

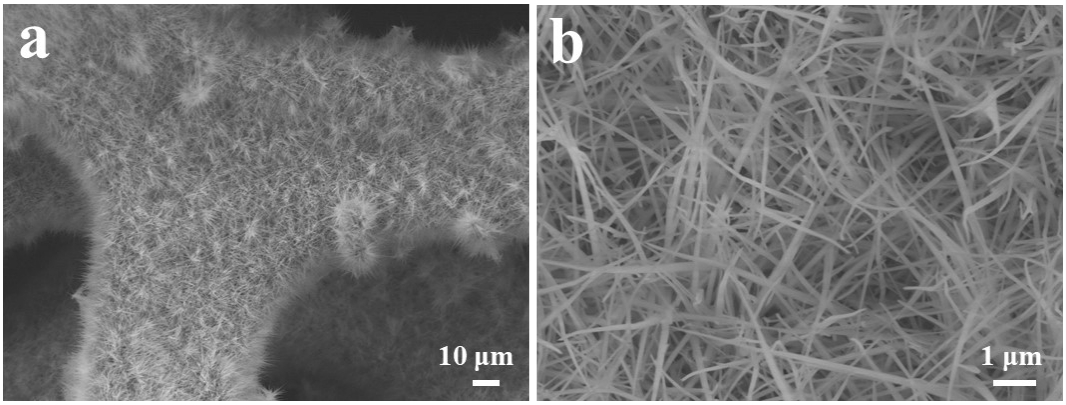

Figure S4. SEM images of (a) low magnification and (b) high magnification of $NiMoO_4$ precursor.

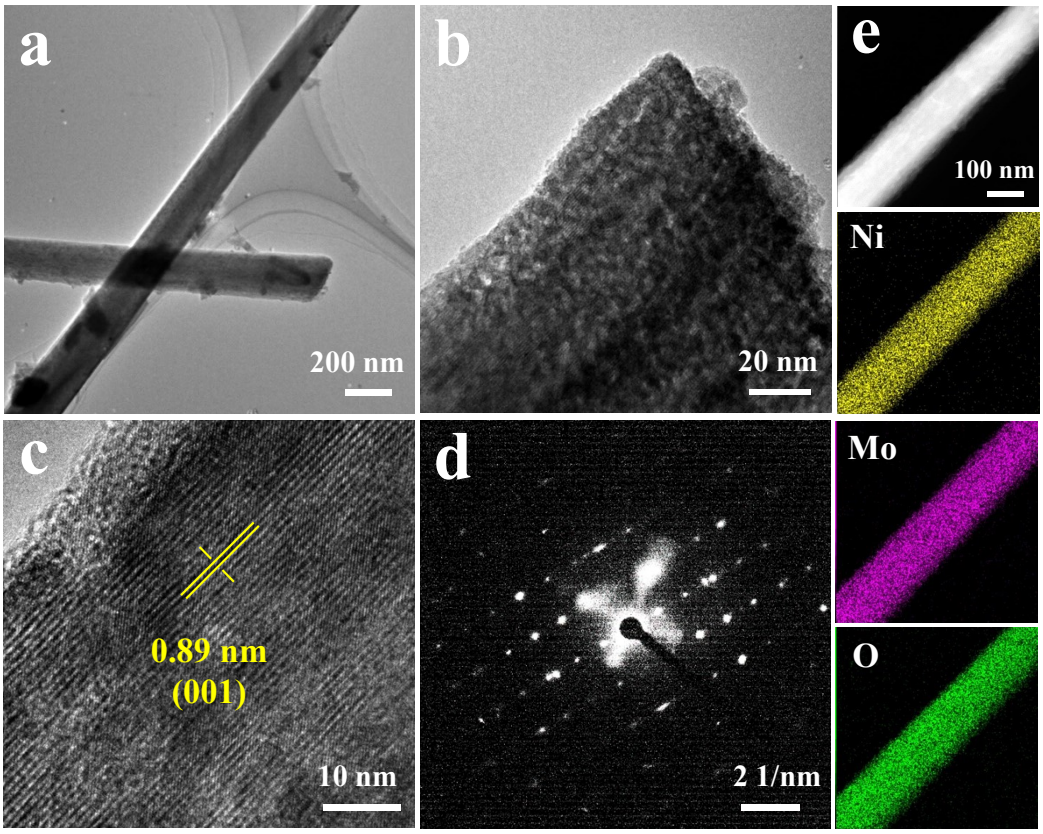

Figure S5 TEM, HRTEM image, HAADF-STEM image and corresponding elemental mappings of the $NiMoO_4$ precursor.

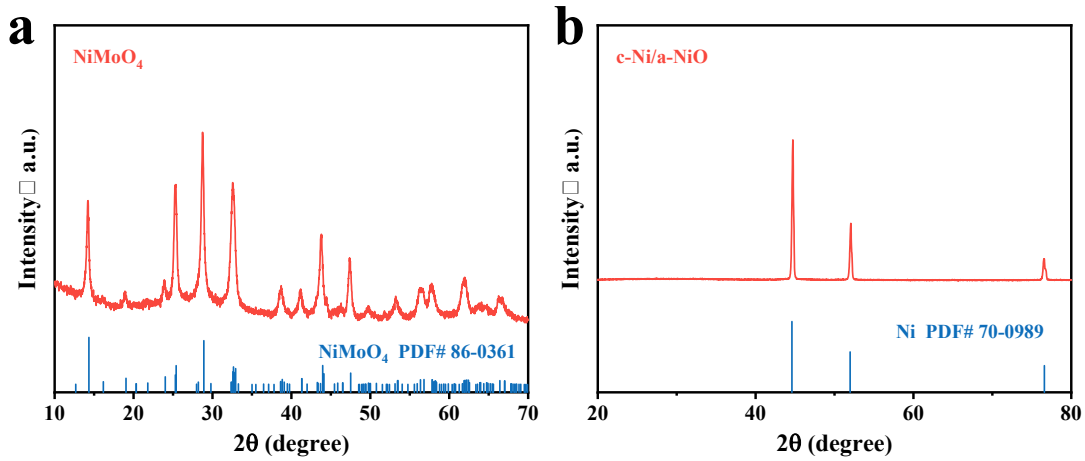

Figure S6. XRD patterns of (a) $NiMoO_4$ and (b) c-Ni/a-NiO.

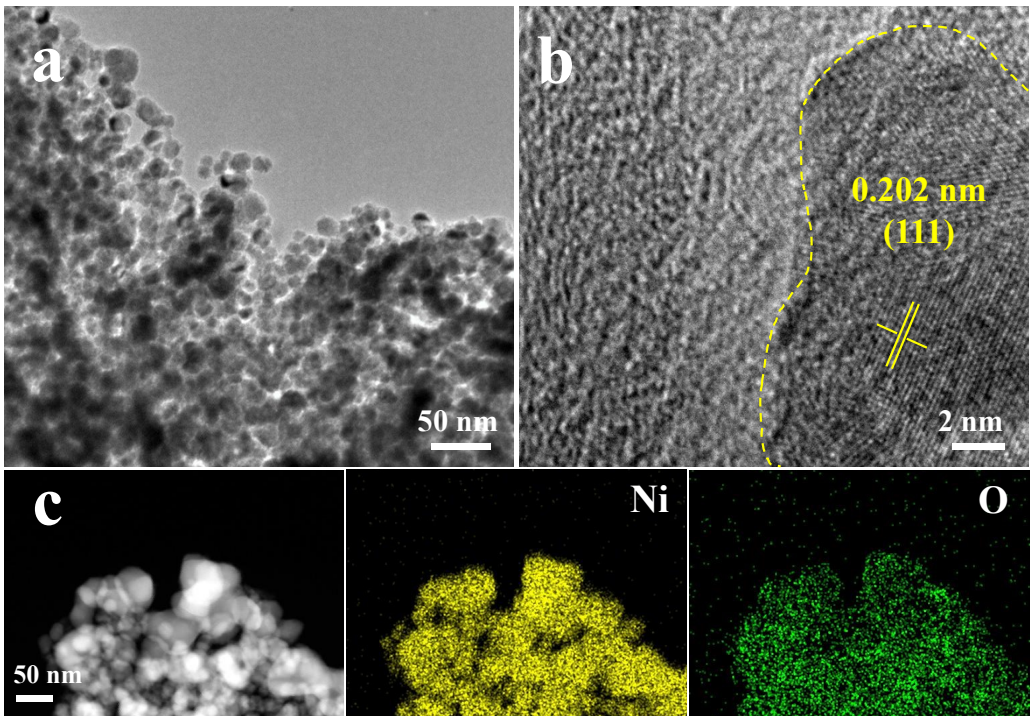

Figure S7. TEM, HRTEM image, HAADF-STEM image and corresponding elemental mappings of the c-Ni/a-NiO catalyst.

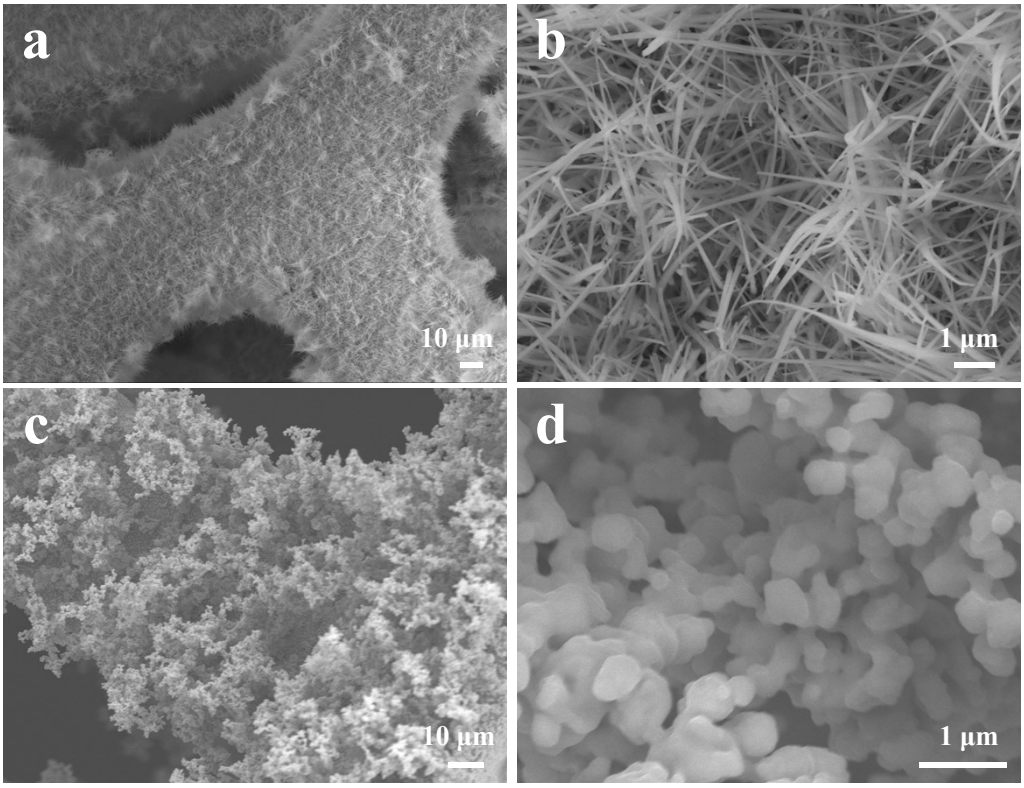

Figure S8. SEM images of (a, b) $NiMoO_4$ and (c, d) c-Ni/a-NiO.

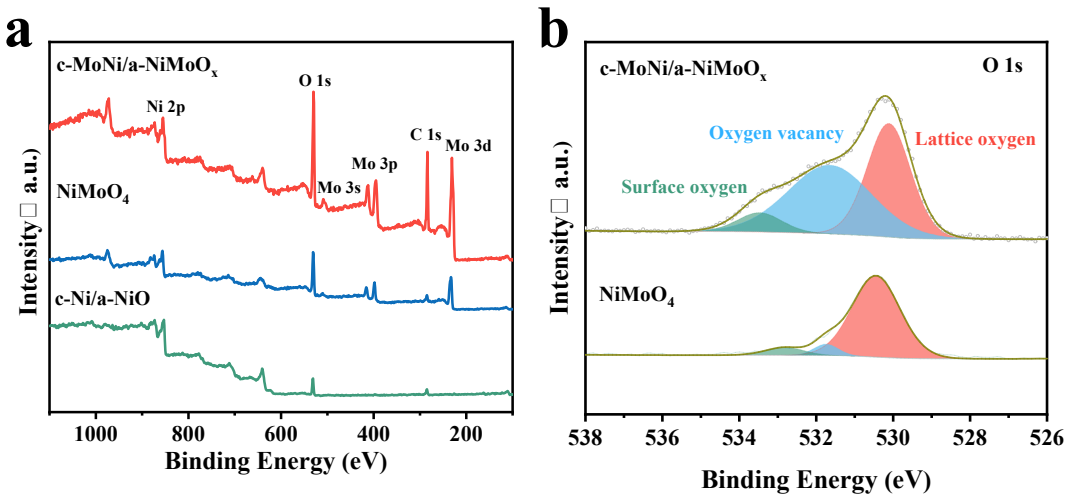

Figure S9. (a) XPS survey spectra of c-NiMo/a-NiMoO$_x$, NiMoO$_4$ and c-Ni/a-NiO. (b) The high-resolution XPS spectra of O of the prepared catalysts.

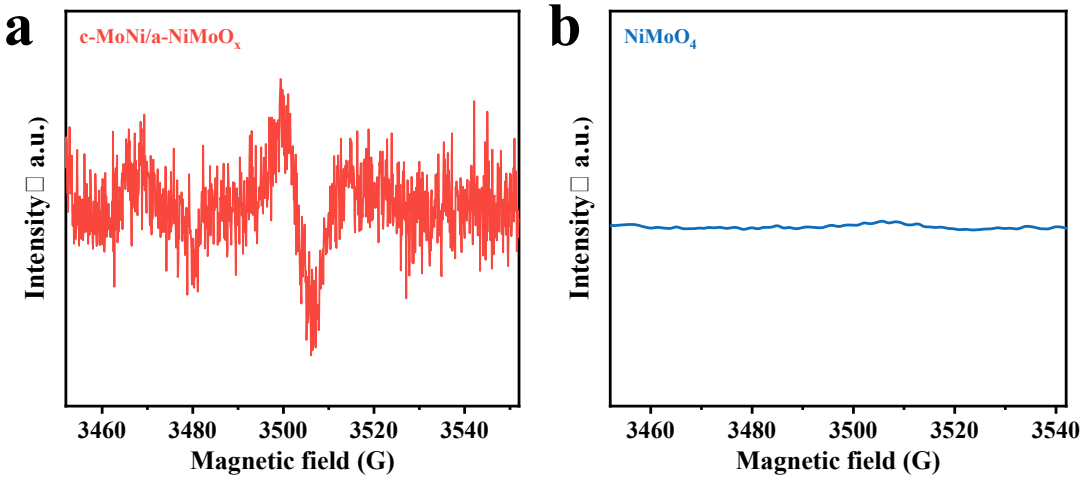

Figure S10. The narrow-band EPR spectra of c-NiMo/a-NiMoO$_x$ and NiMoO$_4$.

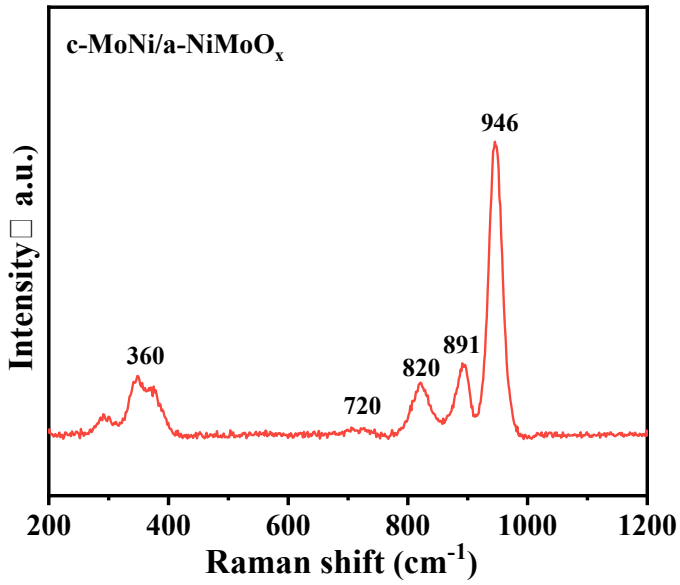

Figure S11. Raman spectra of c-MoNi/a-NiMoO$_x$.

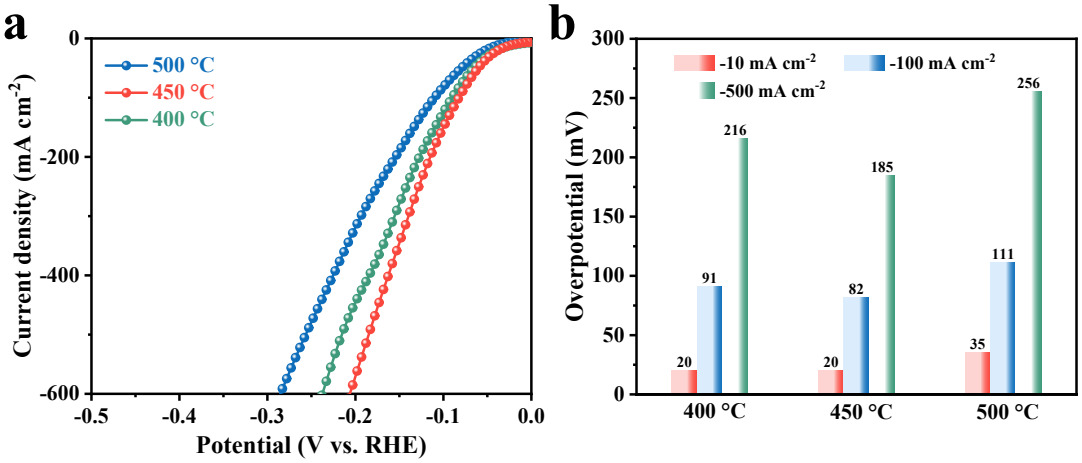

Figure S12. (a) LSV and (b) HER overpotentials at 10/100/500 mA cm^{-2} for $NiMoO_4$ precursors annealed at different temperatures.

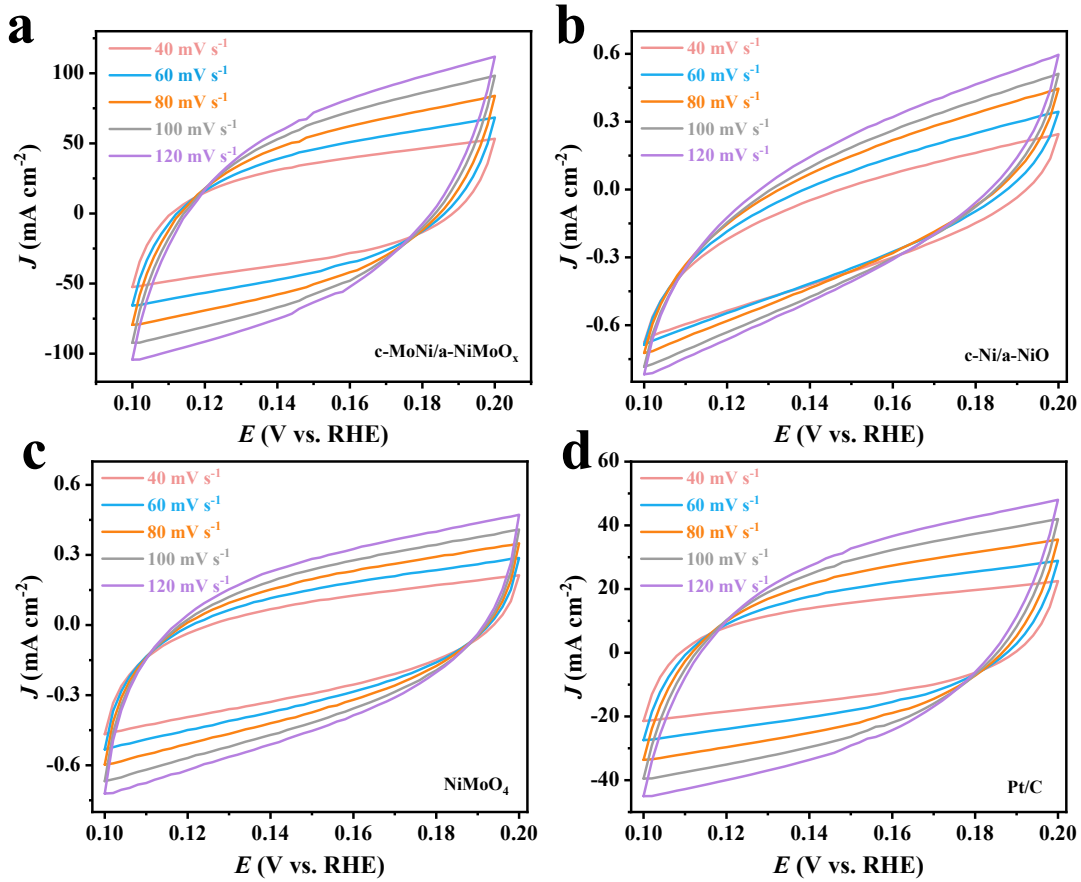

Figure S13. CV curves of (a) c-NiMo/a-$NiMoO_x$, (b) c-Ni/a-NiO, (c) $NiMoO_4$ and (d) Pt/C in the non-faradaic region.

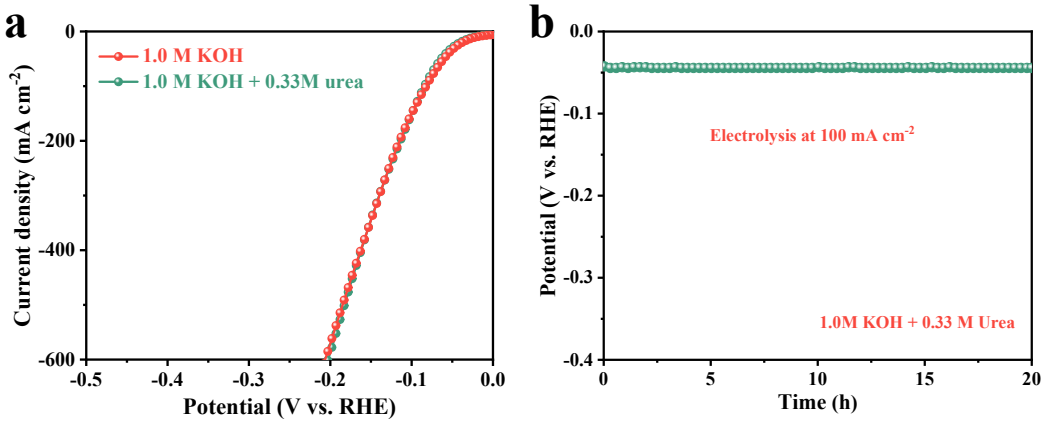

Figure S14. (a) HER polarization curves of c-MoNi/a-$NiMoO_x$ in 1.0 M KOH and 1.0 M KOH + 0.33 M Urea. (b) Chronopotentiometry test of c-MoNi/a-$NiMoO_x$ in 1.0 M KOH + 0.33 M Urea.

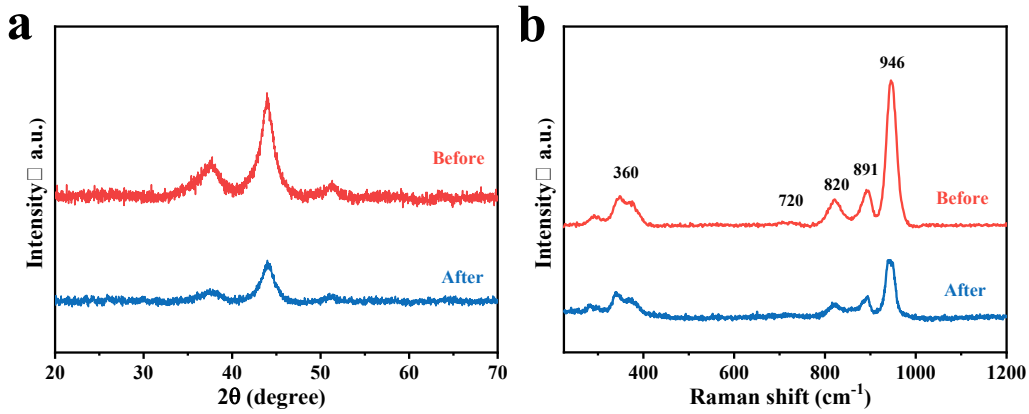

Figure S15. (a) XRD and (b) Raman patterns of c-NiMo/a-$NiMoO_x$ after HER test.

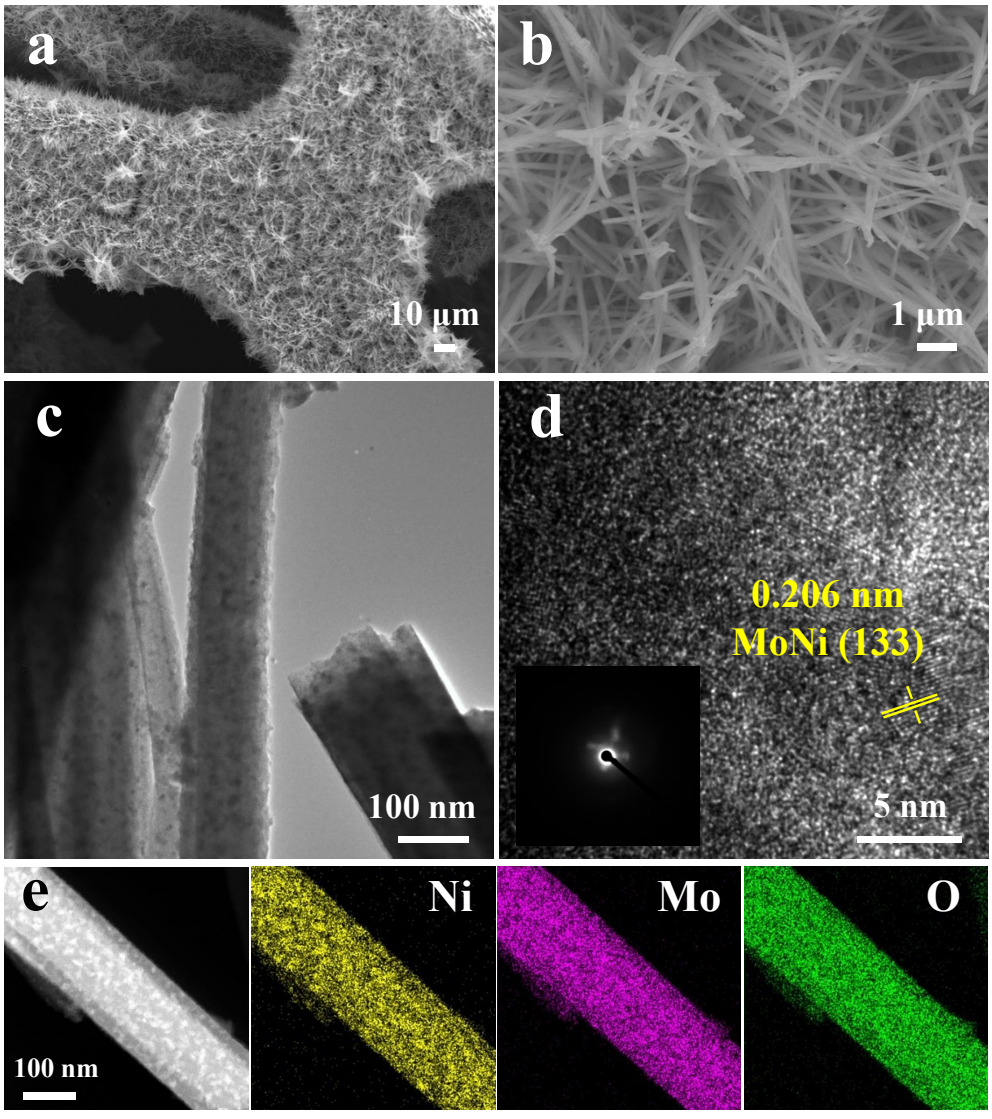

Figure S16. (a, b) SEM images, (c) TEM images, (d) HRTEM images, insets show the SAED pattern, (e) HAADF-STEM image and corresponding elemental mappings of the c-MoNi/a-$NiMoO_x$ after HER test.

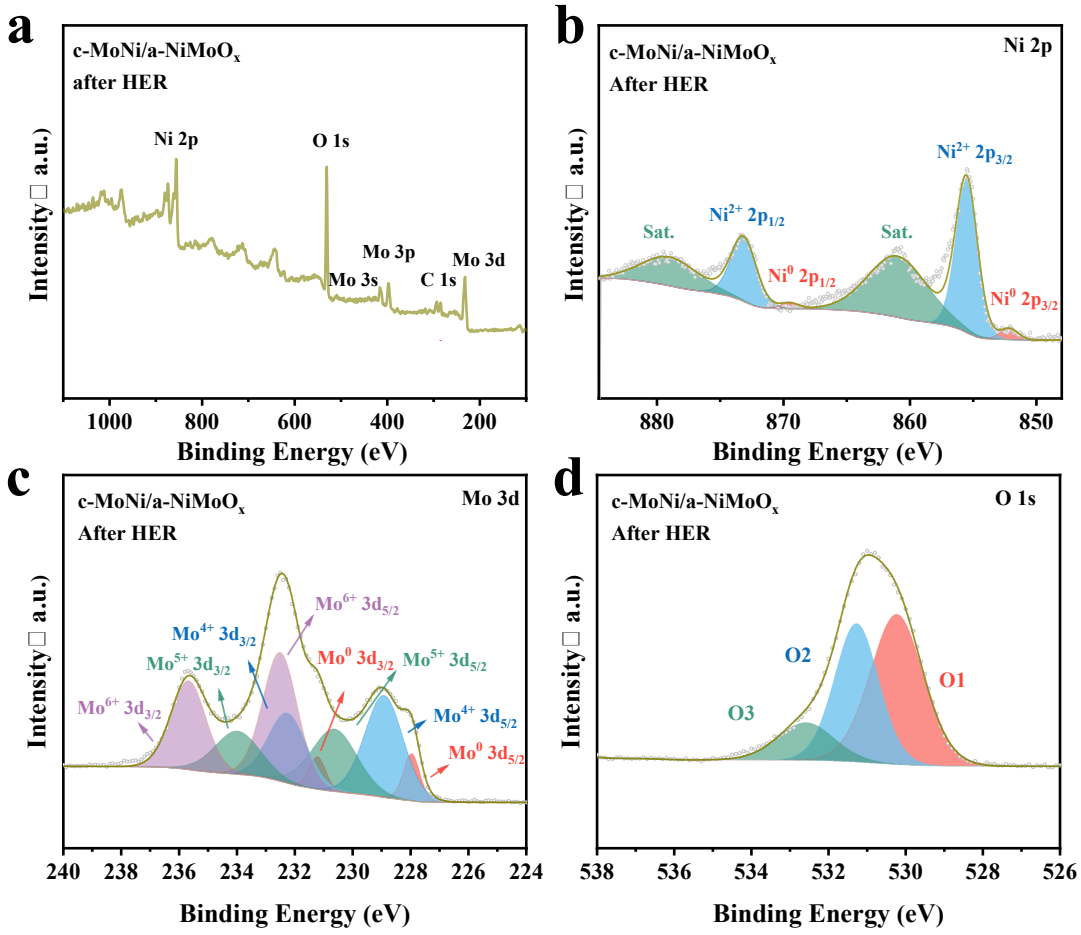

Figure S17. XPS survey spectra (a) and the high-resolution XPS spectra of (b) Ni 2p, (c) Mo 3d and (d) O 1s of c-NiMo/a-NiMoO$_x$ after HER test.

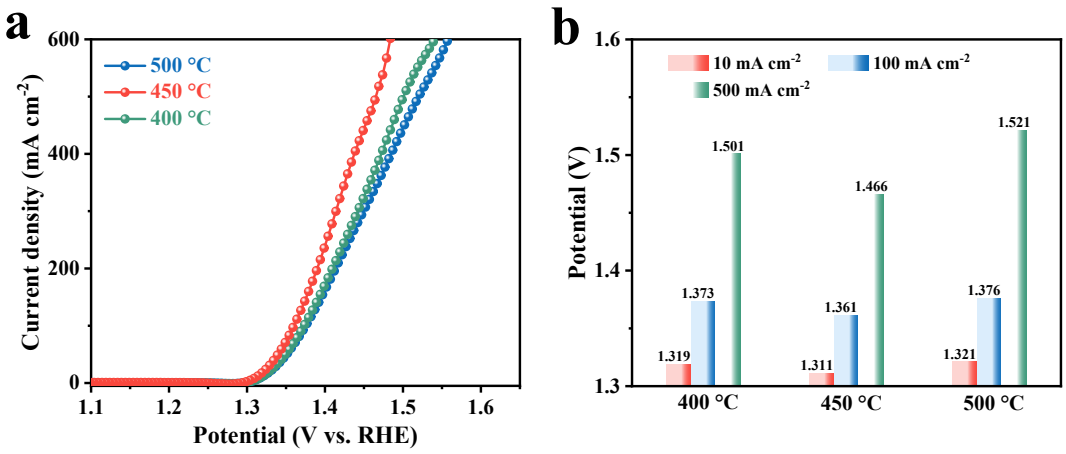

Figure S18. (a) LSV and (b) UOR potentials at 10/100/500 mA cm^{-2} for precursors annealed at different temperatures.

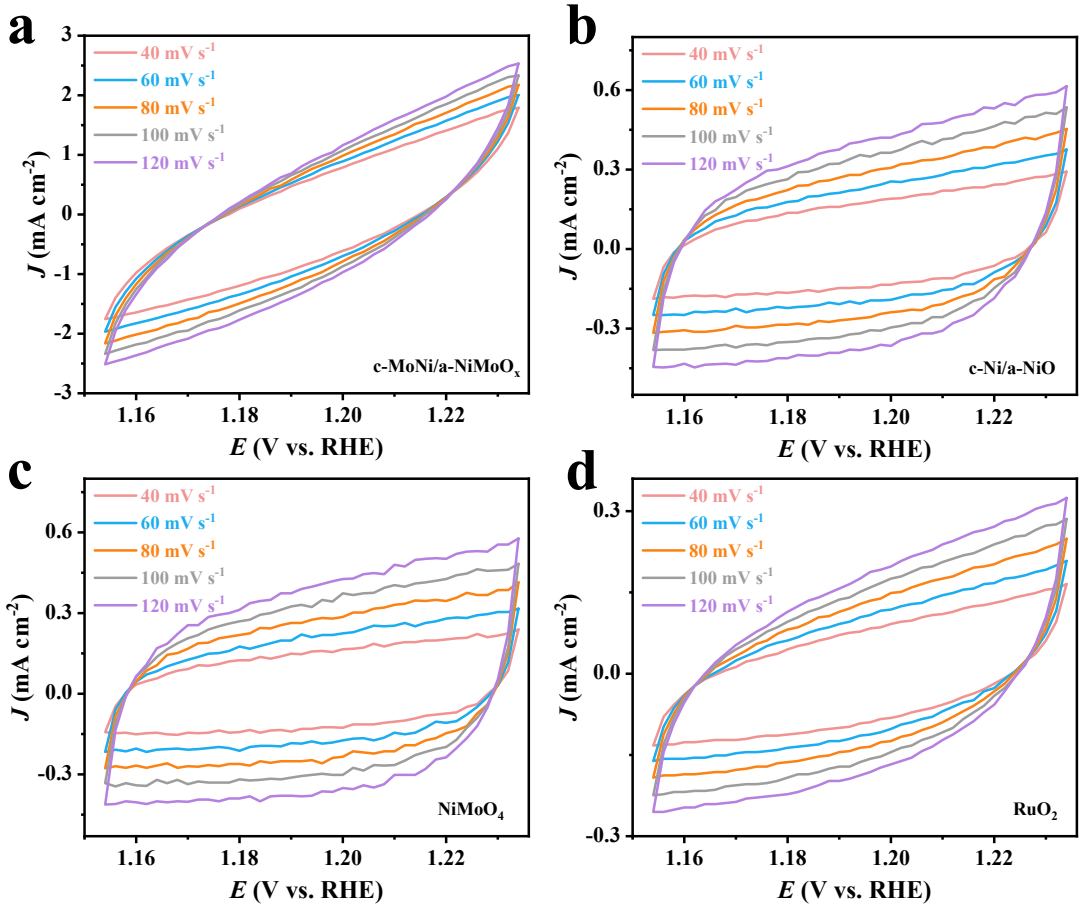

Figure S19. CV curves of (a) c-NiMo/a-$NiMoO_x$, (b) c-Ni/a-NiO, (c) $NiMoO_4$ and (d) Pt/C in the non-faradaic region.

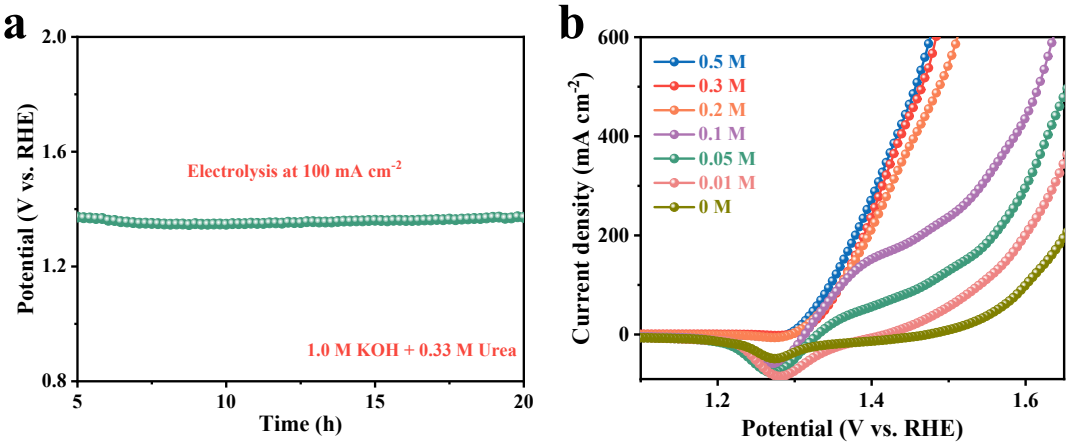

Figure S20. (a) Chronopotentiometry test of c-MoNi/a-$NiMoO_x$ in 1.0 M KOH + 0.33 M Urea. (b) UOR polarization curves of c-MoNi/a-$NiMoO_x$ with different urea contents in 1.0 M KOH.

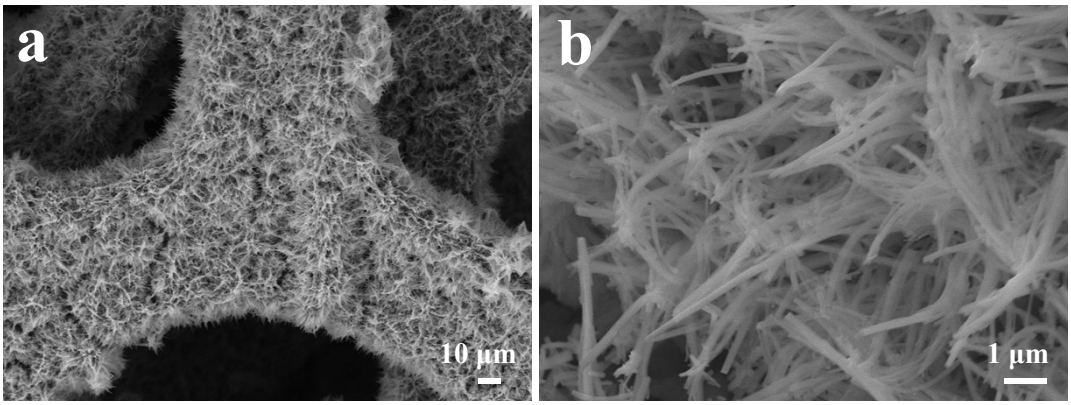

Figure S21. SEM images of the c-NiMo/a-$NiMoO_x$ catalyst after UOR test.

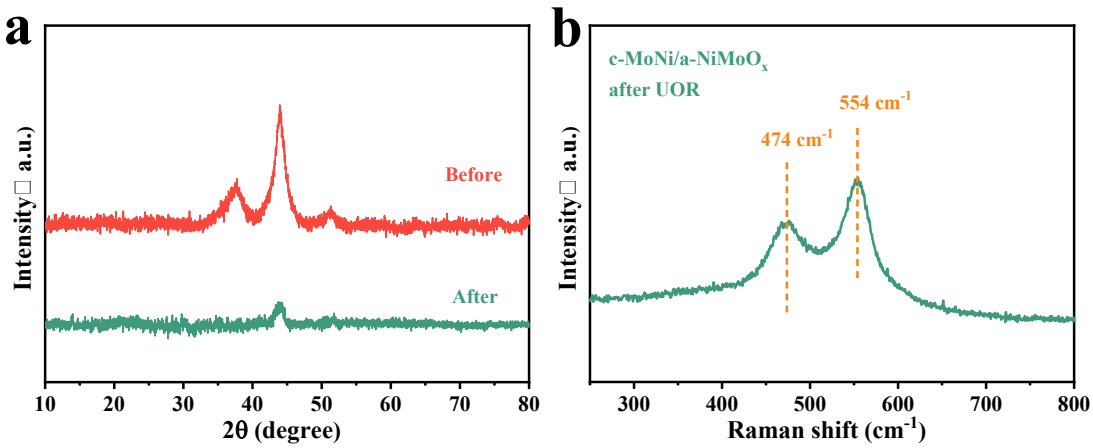

Figure S22. (a) XRD and (b) Raman patterns of c-NiMo/a-$NiMoO_x$ after UOR test.

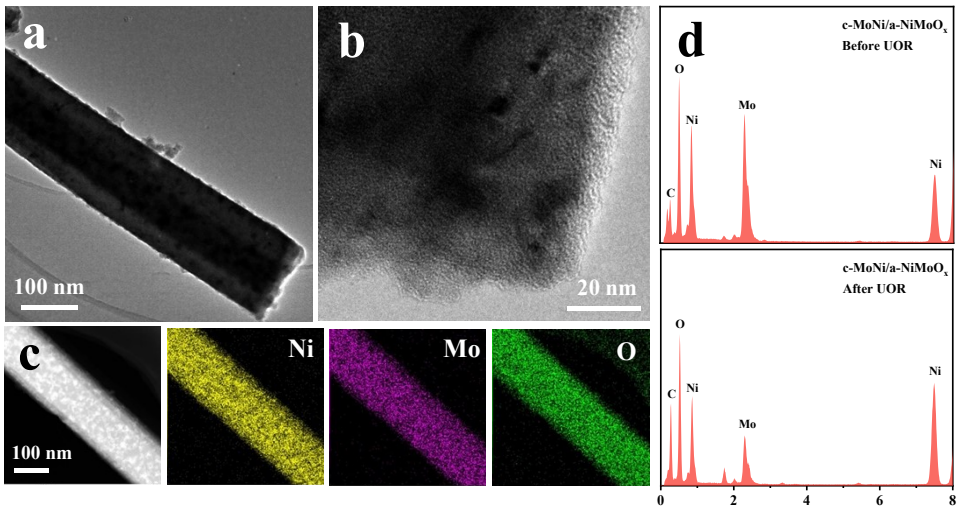

Figure S23. (a, b) TEM images at different magnifications, (c) HAADF-STEM image and corresponding elemental mappings, (d) EDS spectra of c-MoNi/a-NiMoO$_x$ after UOR test.

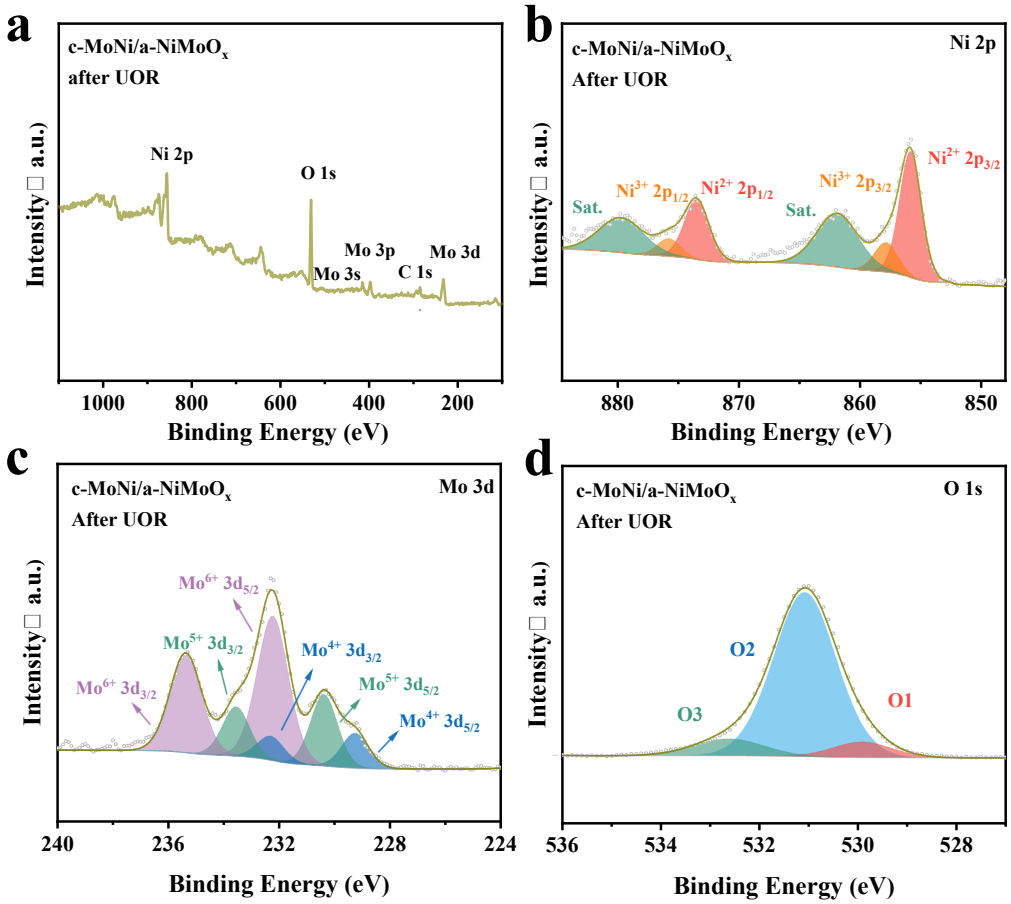

Figure S24. XPS survey spectra (a) and the high-resolution XPS spectra of (b) Ni 2p, (c) Mo 3d, and (d) O 1s of c-NiMo/a-NiMoO$_x$ after UOR test.

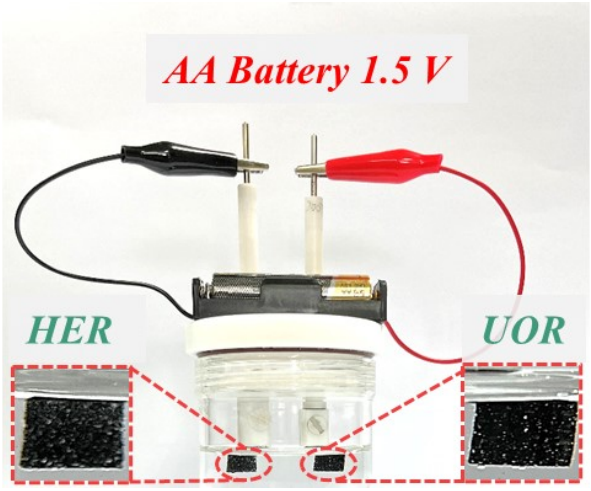

Figure S25. Diagram of urea-assisted water splitting driven by commercial AA batteries.

Figure S26. Diagram of urea-assisted water splitting driven by wind power.

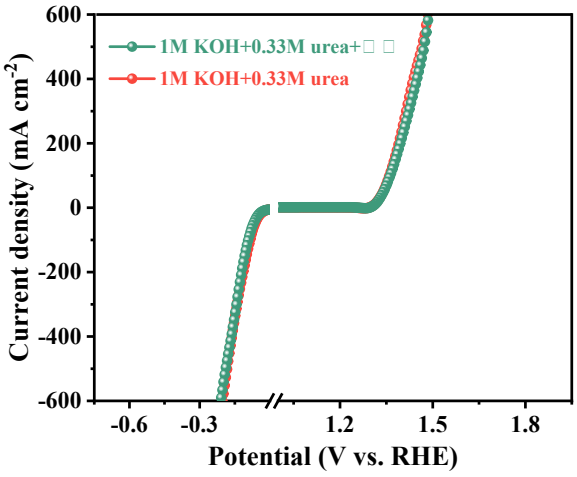

Figure S27. Comparison of HER and UOR polarization curves of c-MoNi/a-$NiMoO_x$ in 1.0 M KOH + 0.33 M Urea and 1 M KOH + 0.33 M Urea + seawater.

Supplementary Tables

Table S1. ICP-OES data for c-MoNi/a-$NiMoO_x$.

Samples	Ni (mg/L)	Mo (mg/L)	actual Ni/Mo atomic ratio
c-MoNi/a-$NiMoO_x$	**6.253**	**1.014**	**1:1**

Table S2. Comparison of the HER activity of c-NiMo/a-$NiMoO_x$ with other reported non-noble-metal electrocatalysts in 1M KOH. η_{-10} is overpotentials required to achieve current densities of 10 mA cm^{-2}.

Catalysts	Electrolyte	η_{-10} (mV)	Reference
c-NiMo/a-$NiMoO_x$	***1.0 M KOH***	***20***	***This work***
Ni(Cu)VO_x	1.0 M KOH	21	*Nat. Commun.*, 2020, 11, 2720.
Ni_2P/NiMoP	1.0 M KOH	22	*eScience*, 2021, 1, 69-74.
$Cu_{0.5}Ni_{0.5}$	1.0 M KOH	28	*Small*, 2023, 19, 2300959.
Fe_2P@Ni_xP	1.0 M KOH	33	*Chem. Eng. J.*, 2021, 417, 128067.
$Ni(OH)_2$-$NiMoO_x$	1.0 M KOH	36	*Adv. Energy Mater.*, 2019, 9, 1902703.
Ni_2PCoCH	1.0 M KOH	62	*Angew. Chem. Int. Ed.*, 2023, 62, e202302795.
W_1Mo_1-NG	1.0 M KOH	67	*Sci. Adv.*, 2020, 6, eaba6586.
Co_xMo_yCH	1.0 M KOH	82	*J. Energ. Chem.*, 2022, 70, 258-265.
N-WS_2/Ni_3FeN	1.0 M KOH	84	*Small*, 2022, 18, 2104624.
Ni_2P-$NiMoO_x$	1.0 M KOH	91	*ACS Catal.*, 2023, 13, 97929805.

Fe-Mo-S/Ni_3S_2	1.0 M KOH	144	*Chem. Eng. J.*, 2021, 404, 126483.

Table S3. Comparison of the UOR activity of c-NiMo/a-$NiMoO_x$ with other reported non-noble-metal electrocatalysts in urea-rich 1.0 M KOH.

Catalysts	Urea concentration	Voltage (E_{10}, V)	Reference
c-NiMo/a-$NiMoO_x$	***0.33 M Urea***	***1.31***	***This work***
Ni_3N/Mo_2N	0.33 M Urea	1.32	*ACS Catal.*, 2023, 13, 4091-4100.
$Cu_{0.5}Ni_{0.5}$	0.5 M Urea	1.33	*Small*, 2023, 2300959.
Co_xMo_yCH	0.33 M Urea	1.33	*J. Energy Chem.*, 2022, 70, 258-265.
Ni/W_5N_4	0.5 M Urea	1.34	*Appl. Catal. B: Environ.*, 2023, 323, 122168.
Fe_2P@Ni_xP	0.5 M Urea	1.35	*Chem. Eng. J.*, 2021, 417, 128067.
$NiSe_2/MoSe_2$	0.5 M Urea	1.34	*Appl. Catal. B: Environ.*, 2024, 341, 123312.
$Ni_2P_4O_{12}$/NiTe	0.33 M Urea	1.34	*Adv. Mater.*, 2024, 36, 2311766.
Ni-WO_x	0.33 M Urea	1.40	*Angew. Chem. Int. Ed.*, 2021, 60, 10577.
NiS/MoS_2@CC	0.5 M Urea	1.36	*Chem. Eng. J.*, 2022, 443, 136321.
O_{vac}-V-$Ni(OH)_2$	0.33 M Urea	1.47	*Adv. Funct. Mater.*, 2022, 33, 2209698.

Table S4. Comparison of overall urea splitting performance of c-NiMo/a-$NiMoO_x$ with other reported bifunctional electrocatalysts in urea-rich 1.0 M KOH.

Catalysts	Urea concentration	Cell voltage（E_{10}, V）	Reference
c-NiMo/a-$NiMoO_x$	***0.33 M Urea***	***1.327***	***This work***
Ni_3N/Mo_2N	0.33 M Urea	1.36	*ACS Catal.*, 2023, 13, 4091.
$Ni_2P_4O_{12}$/NiTe	0.33 M Urea	1.37	*Adv. Mater.*, 2024, 2311766.
F-NiO/Ni@C	0.33 M Urea	1.37	*Adv. Funct. Mater.*, 2023,33, 2303986.
a-RuO_2/NiO	0.33 M Urea	1.372	*ACS Nano*, 2024, 18, 1214-1225.
$Cu_{0.5}Ni_{0.5}$	0.5 M Urea	1.38	*Small*, 2023, 19, 2300959.
Co_xMo_yCH	0.33 M Urea	1.40	*J. Energy Chem.*, 2022, 70, 258-265.
N-Co_9S_8/Ni_3S_2	0.5 M Urea	1.40	*Small*, 2023, 19, 2207425.
$NiSe_2/MoSe_2$	0.5 M Urea	1.44	*Angew. Chem. Int. Ed.*, 2021, 60, 10577-10582.
NiS/MoS_2@CC	0.5 M Urea	1.46	*Chem. Eng. J.*, 2022, 443, 136321.

Supplementary references

1 G. Kresse and J. Furthmüller, *Comp. Mater. Sci.*, 1996, 6, 15-50.

2 G. Kresse and J. Furthmüller, *Phys. Rev. B*, 1996, 54, 11169-11186.

3 J. P. Perdew, K. Burke and M. Ernzerhof, *Phys. Rev. Lett.*, 1996, 77, 3865-3868.

4 G. Kresse and D. Joubert, *Phys. Rev. B*, 1999, 59, 1758-1775.

5 P. E. Blöchl, *Phy. Rev. B*, 1994, 50, 17953-17979.

6 S. L. Dudarev, G. A. Botton, S. Y. Savrasov, C. J. Humphreys and A. P. Sutton, *Phy. Rev. B*, 1998, 57, 1505-1509.

7 S. Grimme, J. Antony, S. Ehrlich and H. Krieg, *J. Chem. Phys.*, 2010, 132, 154104.